Time-Resolved Absorption and Emission Show that the CP43′ Antenna Ring of Iron-Stressed *Synechocystis* sp. PCC6803 Is Efficiently Coupled to the Photosystem I Reaction Center Core[†,‡]

Alexander N. Melkozernov,[§] Thomas S. Bibby,[||] Su Lin,[§] James Barber,[||] and Robert E. Blankenship*[,§]

Department of Chemistry and Biochemistry and Center for the Study of Early Events in Photosynthesis, Arizona State University, Tempe, Arizona 85287-1604, and Wolfson Laboratories, Department of Biological Sciences, Imperial College of Science, Technology & Medicine, London SW7 2AY, U.K.

Received October 10, 2002; Revised Manuscript Received January 13, 2003

ABSTRACT: Excitation energy transfer and trapping processes in an iron stress-induced supercomplex of photosystem I from the cyanobacterium *Synechocystis* sp. PCC6803 were studied by time-resolved absorption and fluorescence spectroscopy on femtosecond and picosecond time scales. The data provide evidence that the energy transfer dynamics of the CP43′−PSI supercomplex are consistent with energy transfer processes that occur in the Chl *a* network of the PSI trimer antenna. The most significant absorbance changes in the CP43′−PSI supercomplex are observed within the first several picoseconds after the excitation into the spectral region of CP43′ absorption (665 nm). The difference time-resolved spectra ($\Delta\Delta A$) resulting from subtraction of the PSI trimer kinetic data from the CP43′−PSI supercomplex data indicate three energy transfer processes with time constants of 0.2, 1.7, and 10 ps. The 0.2 ps kinetic phase is tentatively interpreted as arising from energy transfer processes originating within or between the CP43′ complexes. The 1.7 ps phase is interpreted as possibly arising from energy transfer from the CP43′ ring to the PSI trimer via closely located clusters of Chl *a* in CP43′ and the PSI core, while the slower 10 ps process might reflect the overall excitation transfer from the CP43′ ring to the PSI trimer. These three fast kinetic phases are followed by a 40 ps overall excitation decay in the supercomplex, in contrast to a 25 ps overall decay observed in the trimer complex without CP43′. Excitation of Chl *a* in both the CP43′−PSI antenna supercomplex and the PSI trimer completely decays within 100 ps, resulting in the formation of $P700^+$. The data indicate that there is a rapid and efficient energy transfer between the outer antenna ring and the PSI reaction center complex.

Through the process of photosynthesis, cyanobacteria are major producers of oxygen in the Earth's biosphere. During adaptive evolution, this group of photosynthetic microorganisms acquired different survival strategies, resulting in a dynamic rearrangement of the light-harvesting antenna supplying the photosynthetic machinery of photosystem II (PSII)[1] and photosystem I (PSI) with solar energy (*1*). One example of the regulation of light harvesting capacity involves changes in the extent and structure of phycobilisomes that allow cyanobacteria and red algae to respond to their environmental conditions (*2*, *3*). Such a response occurs when cyanobacteria are exposed to a limiting supply of iron, a common occurrence in their natural environment (*4*). Under iron stress conditions, there is a significant lowering of the phycobiliprotein content (*5*) and overall reduction of the photosystem I (PSI) level relative to that of photosystem II (PSII) (*6*). These changes seem, in part, to be compensated by the accumulation of the IsiA protein (CP43′) encoded by the "iron stress-induced" *isi*A gene (*7*−*9*), which is a Chl *a*-binding protein with amino acid sequence and topology similar to those of the CP43 protein of PSII (*10*, *11*). Because of this similarity with CP43, the iron stress protein was suggested to be associated with PSII functioning as a Chl storage protein (*9*) or an excitation energy dissipator (*5*, *12*).

Recently, a supercomplex composed of CP43′ and the PSI reaction center trimer, with a molecular mass of approximately 2000 kDa, has been biochemically isolated from the cyanobacterium *Synechocystis* sp. PCC6803 (*10*, *13*). A single-particle analysis of electron microscopy images showed that in iron-stressed cells the CP43′ protein is structurally associated with the PSI complex as a ring around the PSI trimer. The available X-ray structures of the cyanobacterial PSI trimer (*14*) and of CP43 from a PSII complex (*15*) have

[†] This work was supported by NSF Grant MCB-9727607 to R.E.B., NRICGP/USDA Grant 2001-35318-11110 to A.N.M., and a BBSRC grant to J.B.

[‡] This is publication 557 of the Center for the Study of Early Events in Photosynthesis at Arizona State University.

* To whom correspondence should be addressed: Department of Chemistry and Biochemistry, Arizona State University, Tempe, AZ 85287-1604. Phone: (480) 965-1439. Fax: (480) 965-2747. E-mail: Blankenship@asu.edu.

[§] Arizona State University.

[||] Imperial College of Science, Technology & Medicine.

[1] Abbreviations: Chl *a*, chlorophyll *a*; CP43, PsbC subunit of photosystem II; CP43′, iron stress-induced protein encoded by the *isi*A gene; ΔA, absorbance change; cryo-EM, electron cryomicroscopy; DAS, decay-associated spectrum; FDAS, fluorescence decay-associated spectrum; fwhm, full width at half-maximum; IRF, instrument response function; ND, nondecaying component; PB, photobleaching; PSI, photosystem I; PSII, photosystem II; P700, primary electron donor in photosystem I; RC, reaction center; SE, stimulated emission; SPC, single-photon counting.

10.1021/bi026987u CCC: $25.00
Published on Web 03/14/2003

been satisfactorily modeled into a three-dimensional (3D) structure of the CP43′−PSI supercomplex derived from electron cryomicroscopy (*16*). On the basis of this structure and earlier modeling (*10*, *13*), the CP43′ ring was shown to be composed of 18 copies of the protein. If each CP43′ binds ∼12 Chl *a* molecules as does CP43 (*15*), then the extra ring would increase the light harvesting capacity of PSI by 72%. Similar findings have been reported for the cyanobacterium *Synechococcus* sp. PCC7942 (*17*) and the oxyphotobacterium *Prochlorococcus marinus* (*18*), indicating that the observed phenomenon might be an example of a different survival strategy in the adaptive evolution of the photosynthetic supercomplexes. It seems likely that the formation of the CP43′ ring occurs to extend the absorption cross section of the PSI reaction center (RC), thus compensating for the lack of PSI and phycobilisomes under low-iron conditions (*10*, *13*, *17*).

Spectroscopic studies of the past decade showed that cyanobacterial PSI very efficiently converts solar energy into the electrochemical potential energy of the charge separation in the PSI (*17*−*21*). The current 2.5 Å resolution structure of the PSI trimer from the cyanobacterium *Synechococcus elongatus* (*14*, *22*) reveals a network of ∼100 Chl *a* molecules arranged in each PSI monomer as an irregular sphere around the reaction center. The main structural feature of the network is that both core antenna Chls and the cofactors of the RC are bound to the same PsaA−PsaB heterodimer. In addition to the PsaA−PsaB dimer that binds the majority of the Chls, there are 10 additional protein subunits attached to each PSI monomer. Four of them (PsaX, PsaJ, PsaL, and PsaK) bind Chl *a* (*14*, *23*). In the thylakoids of chloroplasts, the PSI complexes are assembled as trimers where monomeric PSI is coupled via the trimer-forming domain containing the PsaL subunit.

Time-resolved studies of the PSI trimers from different cyanobacteria reported two major phases of energy transfer with lifetimes of 0.2−0.5 and 2−4 ps (*24*−*27*). The subpicosecond phase reflects the spectral equilibration in the bulk antenna where the majority of the Chls are involved in the network of singlet excitation energy transfer between closely located neighbors. On the longer time scale, the equilibration process involves all Chl *a* spectral forms, including the long wavelength-absorbing species (red pigments). The number of long wavelength-absorbing Chls is species-dependent, which results in some differences in the excitation dynamics. Energy equilibration processes longer than 2−4 ps have been reported for the PSI trimers from *S. elongatus* and *Spirulina platensis* (*19*, *21*), suggesting that some additional long wavelength-absorbing species might participate in energy equilibration within the PSI trimer. However, for PSI from the cyanobacterium *Synechocystis* sp. PCC6803, the excitation dynamics in the trimers and monomers are very similar, reflecting the relatively small amount (approximately two Chl *a* dimers) of red pigment in this species (*20*, *25*).

The excitation equilibrated in the PSI trimer antenna on the picosecond time scale is trapped by the reaction center within 20−25 ps in *Synechocystis* sp. PCC6803 and within 30−50 ps in *S. elongatus* and *Sp. platensis* (*19*−*21*). The energy equilibration phases and trapping in the CP43′−PSI supercomplex have not previously been reported. Comparison of the 77 K steady state fluorescence of the PSI supercomplex and the PSI trimer (*13*) indicates that most of the CP43′ efficiently transfers energy to the PSI reaction center core. Analysis of the cryo-EM structural model of the supercomplex suggests that for each PSI monomer in the supercomplex there are three regions where the Chls in CP43′ are located closer to Chl *a* clusters in PsaA, PsaB, and PsaJ with interpigment distances of ∼20−25 Å (*10*, *16*). A recent study of the excitation dynamics in isolated CP43 from higher plants, which is thought to be similar in structure to the CP43′, reported two spectral relaxation phases with lifetimes of 0.2−0.4 and 2−3 ps (*28*). The available 3.8 Å resolution structure of the PSII complex (*15*) models CP43 as three pairs of transmembrane helices binding 12 Chl *a* molecules. Two separate clusters of the Chls form layers toward the stromal and lumenal surfaces of the protein. Interpigment distances among these 12 Chls vary from 9.8 to 33 Å. If it is assumed that CP43′ binds Chls in the same way as CP43, then the tight interactions between the CP43′ subunits in the antenna ring of the supercomplex indicate that the Chls in adjacent subunits can be as little as 10 Å from each other (*16*). The well-studied LH2−LH1−RC supercomplex in purple bacteria is an example of the light-harvesting strategy based on the ring structure of the BChl-binding polypeptides (*29*, *30*). In the rings (both LH2 and LH1), the specific structure of the proteins and the arrangement of the chromophores determine the ultrafast delocalization of the excitation energy throughout the ring. Distances between LH2 and LH1 rings enable a picosecond energy transfer, while the distance from the LH1 ring to the RC is a limiting step in the energy transfer. In purple bacteria, this process takes 35 ps to reach the reaction center, thus making the bacterial supercomplex dynamics limited by transfer to trap. A similar model was suggested for the excitation dynamics in the PSI core from cyanobacteria (*21*); however, a series of data for PSI from *Synechocystis* sp. PCC6803 and *Chlamydomonas reinhardtii* support the trap-limited model (*25*, *31*, *32*). In the trap-limited mechanism, excitations may make multiple visits to the trap before photochemical quenching by the reaction center. The observed 20−25 ps trapping time in the PSI reaction center depends on both the effective antenna size and the intrinsic rate of electron transfer from the excited primary electron donor, special pair P700*. Recent structure-based modeling, however, indicates that the excited state dynamics in the PSI core antenna are neither pure trap-limited nor purely limited by transfer to trap but rather balanced (*33*).

In this paper, we present an energy transfer study of the CP43′−PSI supercomplex formed in the cells of the cyanobacterium *Synechocystis* sp. PCC6803 under iron deficiency conditions. Using time-resolved absorption and fluorescence spectroscopy, we show that the ring of the Chl *a*-binding CP43′ antenna is energetically strongly coupled to the PSI trimer. Our results indicate that the outer antenna ring complements the efficient Chl *a* network of the PSI reaction center core in a way that the excitation energy equilibration between CP43′ and the PSI core antenna is faster than the lifetime of the excitation trapping in the whole supercomplex.

MATERIALS AND METHODS

Isolation of PSI Trimers and PSI Supercomplexes. Cells of the cyanobacterium *Synechocystis* sp. PCC6803 having a histidine tag engineered into the carboxy terminus of the PSII

Chl *a*-binding protein CP47 (*34*) were grown in the presence of iron (normal conditions) and in the absence of iron (iron-stressed cells) as described previously (*10*, *13*). Thylakoid membranes were isolated, treated with β-dodecyl maltoside, and depleted of His-tagged PSII complexes using procedures published previously (*10*, *13*). Fractions of PSI trimers and CP43′−PSI supercomplexes were isolated by sucrose gradient centrifugation (*10*, *13*).

Transient Absorption Spectroscopy. For time-resolved absorption spectroscopy, the samples were resuspended in 50 mM Mes-NaOH (pH 6.0), 0.5 M betaine, 5 mM $CaCl_2$, 2.5 mM $MgCl_2$, 0.03% β-dodecyl maltoside, 20 mM sodium ascorbate, and 40 μM PMS. The sample was loaded in a spinning cell with an optical path length of 1.2 mm. The rotating rate of the optical cell (5−8 revolutions/s) and recombination times of reduced acceptors were adjusted to prevent the accumulation of $P700^+$ during the measurements. The absorbance of the sample in the cell was ∼1−1.2 at the peak of the Q_y absorption band.

Transient absorption spectra of the PSI trimers and PSI supercomplexes were measured at room temperature using the femtosecond spectrometer described previously (*25*). The samples were excited at 665 nm with 200 fs laser pulses (fwhm = 5 nm) with an energy of <0.5 μJ or 0.94×10^{14} photons $pulse^{-1}$ cm^{-2}. Mutual orientation of the polarization vectors for pump and probe beams was set at the magic angle (54.7°). Transient absorption spectra have been detected with a 0.095 ps step of the pump−probe delay on a 10 ps time scale and a 2 ps time step in a time window from 10 to 110 ps in the 600−750 nm spectral region. The kinetic data were corrected for dispersion and were analyzed globally on the basis of a model of exponential decay of Chl excited states. The analyses included convolution with the instrument response function of the experimental setup (fwhm = 300 fs). The wavelength plots of initial amplitudes of the exponential components represent decay-associated spectra (DAS) with negative and positive amplitudes corresponding to Chl excitation decay and rise (appearance of new spectral bands), respectively.

Picosecond Fluorescence Spectroscopy. The time-resolved fluorescence of PSI trimers and CP43′−PSI supercomplexes were measured using the time-correlated single-photon counting technique (SPC) (*35*). For room-temperature measurements, samples were diluted in the buffer to a final OD of ∼0.1 cm^{-1}. The samples were excited at 600 nm with ∼10 ps laser pulses and a repetition rate of 7.6 MHz. The intensity of the attenuated laser excitation of less than 5×10^{10} photons cm^{-2} $pulse^{-1}$ was used in all experiments to avoid singlet−singlet annihilation. The fluorescence was selected using a monochromator with a slit width of 4 nm (fwhm) and detected by a Hamamatsu R2809U microchannel plate photomultiplier. The channel resolution of the time−amplitude converter was 6.028 ps. The observed kinetics measured with a 5 or 10 nm step in a 640−780 nm region were deconvoluted with an instrument response function (fwhm ≈ 100 ps) and fitted to a sum of exponentials $\sum A_i \exp(-t/\tau_i)$, where A_i and τ_i are the relative amplitude and lifetime of *i*th exponential component, respectively. The results of a three- or four-component fit were judged by a χ^2 parameter and weighted residuals. The fluorescence kinetics were analyzed globally, and fluorescence decay-associated spectra (FDAS) were constructed as a preexponential component plotted against emission wavelength with positive and negative amplitudes in DAS reflecting a fluorescence decay and a fluorescence rise, respectively. The fit amplitudes were scaled to the steady state fluorescence intensity by setting the sum of the products of the amplitudes and the lifetimes equal to the intensity, $\sum_i A_i\tau_i$, at each detection wavelength.

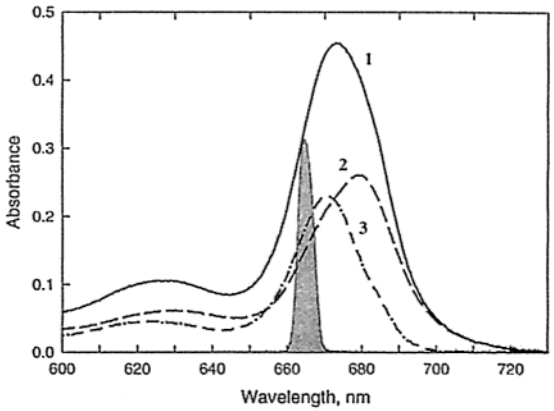

FIGURE 1: Ground state absorption spectra in the region of chlorophyll *a* Q_y transitions of photosystem I complexes isolated from the cyanobacterium *Synechocystis* sp. PCC6803 grown under normal (1, PSI trimers) and iron-stressed (2, CP43′−PSI supercomplex) conditions. A difference spectrum (trace 3, 1 minus 2) indicates a contribution of CP43′ to the Q_y transition of the CP43′−PSI supercomplex. The shaded spectral profile shows the site of the laser excitation at 665 nm (fwhm = 5 nm).

RESULTS

Figure 1 illustrates ground state absorption spectra in the region of Chl *a* Q_y transitions measured at room temperature in the PSI trimers from the normally grown cells of *Synechocystis* sp. PCC6803 (trace 2) and in the CP43′−PSI supercomplexes assembled in the cells grown under iron deficiency conditions (trace 1). The spectra are scaled according to the estimates of the antenna size in an outer ring of the supercomplex based on the available structural model (*10*, *13*, *16*). According to this model, the outer ring of the supercomplex binds ∼216 molecules of the Chl *a*, increasing the antenna size by 72%. The difference spectrum (trace 3) in Figure 1 shows the spectral contribution of CP43′ to the overall absorption spectrum of the supercomplex with the maximum absorption at ∼671 nm. The spectral overlap of the Chl *a* antenna molecules in the PSI supercomplex will significantly complicate the selective excitation of Chl *a* in CP43′. However, the apparent blue shift of the absorption maximum of the PSI supercomplex (673 nm) compared to that of the PSI trimer (680 nm) indicates that excitation at 665 nm is somewhat selective for the outer antenna ring of the supercomplex rather than the Chl *a* species of the PSI trimer. The 665 nm pigments of the PSI trimer core undergo a largely sub-picosecond recovery of the absorption photobleaching upon excitation in this spectral region (*24*, *25*).

Transient Absorption Spectra and Kinetics

PSI Trimers. Figure 2A shows representative transient absorption spectra of the PSI core antenna from *Synechocystis* sp. PCC6803 within 110 ps of excitation at 665 nm. The excitation of the PSI trimers with spectrally narrow (100 cm^{-1}) laser pulses results in an initial decrease in absorption

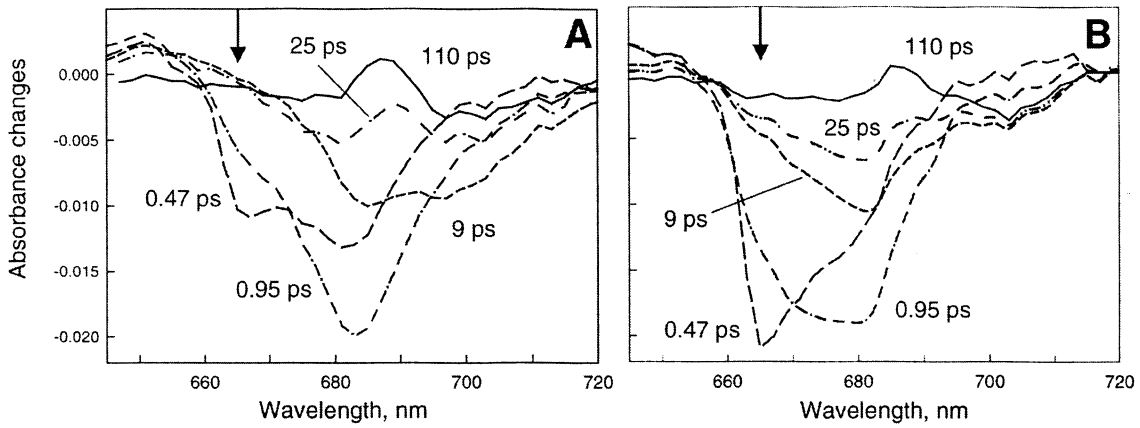

FIGURE 2: Transient difference absorption spectra of the PSI trimer (A) and CP43′−PSI supercomplex (B) measured at 298 K on a 110 ps time scale with excitation at 665 nm (arrow). The spectra are shown at different representative pump−probe delays: 0.47 (− − −), 0.95 (−•−), 9 (- - -), 25 (−••−), and 110 ps (—). The level of spectral noise is ~0.002 Δ*A*.

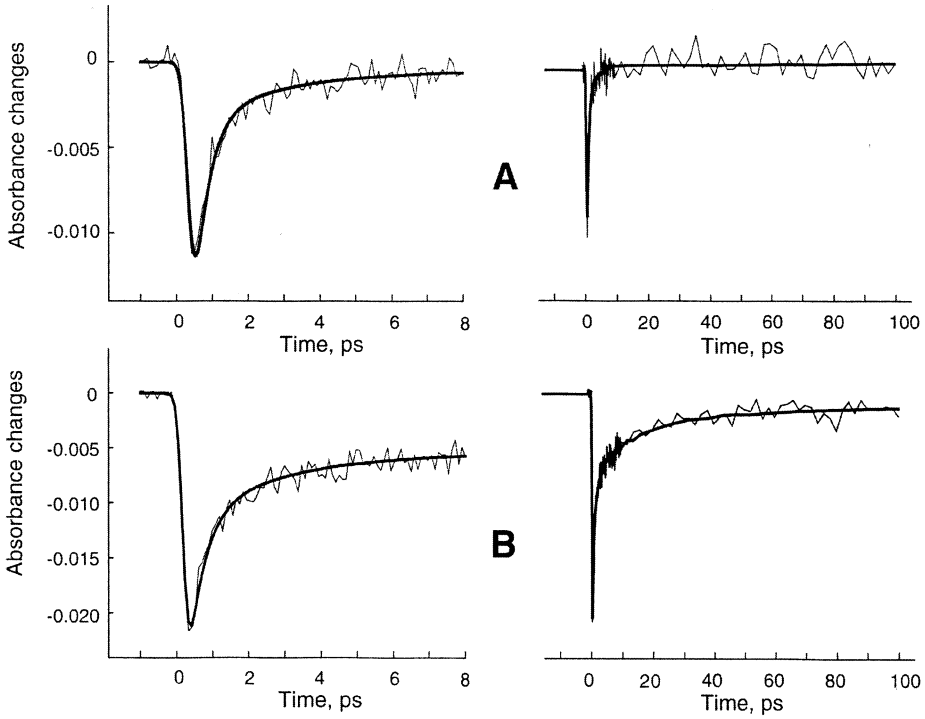

FIGURE 3: Kinetics of the transient absorption changes at 667 nm measured at room temperature induced by excitation at 665 nm in the PSI trimer (A) and CP43′−PSI supercomplex (B) detected on the 8 ps time scale (left) and the 100 ps time scale (right). Solid lines represent the fits of the kinetics based on the three-component exponential model (left panels; see Figure 4) and two-component exponential model (right panels; see Figure 6).

for Chl *a* species at 665 nm due to photobleaching and stimulated emission (PB/SE) in this region. Already at early times, the PB at 665 nm is accompanied by a broad PB band centered at 683 nm, which most probably results from vibronic relaxation of Chl *a* at 683 nm (*25*). However, the 0.47 ps spectrum bears features of the sub-picosecond energy transfer within Chl *a* species as judged by the observed time-dependent increase in the $\Delta A_{683}/\Delta A_{665}$ ratio within 1 ps of the excitation. Transient kinetics at 667 nm in Figure 3A show that in this spectral region decay of PB/SE occurs predominantly on the sub-picosecond time scale. Approximately 1 ps after the excitation (see the 0.95 ps spectrum in Figure 2A), the dominant portion of the Chl *a* excitation centered at 683 nm starts to decay. The shapes of the 0.95 and 9 ps spectra indicate that this decay is overlapped with another spectral shift on the picosecond time scale. The $\Delta A_{683}/\Delta A_{703}$ ratio changes from 4.8 at 0.95 ps to 1.2 at 9 ps, indicative of delayed PB of the spectral band in the region of absorption of long wavelength-absorbing Chl *a* species. The overall decay of the excitation in the PSI trimer antenna occurs on the time scale of tens of picoseconds and represents a trapping of the excitation by the PSI reaction center. A 110 ps spectrum (Figure 2A) indicates a long-lived state resulting from photobleaching of the P700 absorption band due to its $P700^+$ formation in the reaction center. The features of this photobleaching can be seen already in the 25 ps spectrum; however, after the complete decay of the excitation in the core antenna of the PSI trimer, the overall shape of the spectrum remains unchanged until it decays on the millisecond time scale (data not shown).

PSI Supercomplexes. Figure 2B illustrates transient absorption changes of the PB/SE in the PSI supercomplexes

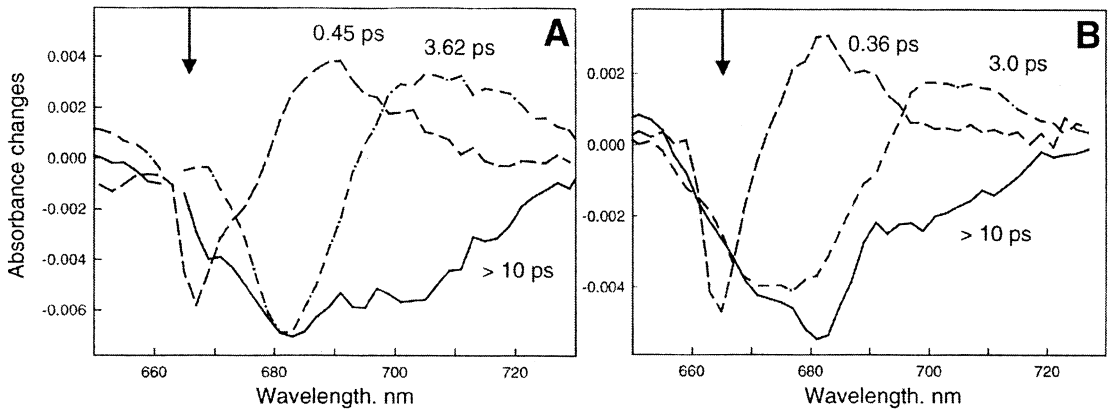

FIGURE 4: Decay-associated spectra (DAS) obtained after global analysis of the transient kinetics detected on the 10 ps time scale with excitation at 665 nm of PSI trimers (A) and the CP43′−PSI supercomplex (B). The data are best fit with three exponential components with lifetimes of 0.3−0.5, 2.5−3.6, and >10 ps. The latter component represents the sum of the excitation trapping and the long-lived P700 photooxidation.

with excitation at 665 nm. The 0.47 ps spectrum is dominated by an asymmetric PB/SE band centered at 665 nm with a broad shoulder at 680 nm. At 0.95 ps, this ΔA band shows a decay at 665 nm; however, in a striking difference from the PSI trimer's transient absorption spectra (Figure 2A), the shape of the 0.95 ps spectrum as well as transient kinetics at 667 nm (Figure 3B) indicates a significant amount of PB in the 660−675 nm spectral region, which decays on a longer time scale. As for the PSI trimer, the overall excitation of the PSI supercomplex starts to decay ∼1 ps after the excitation at 665 nm. However, in the PSI supercomplex, the spectral shifts on the picosecond time scale reveal at least two energy redistribution processes. The $\Delta A_{670}/\Delta A_{681}$ ratio changes from 0.95 in the 0.95 ps spectrum to 0.64 in the 9 ps spectrum. In the PSI trimer, this ratio changes from 0.36 in the 0.95 ps spectrum to 0.08 in the 9 ps spectrum. This is an indication of the energy transfer from CP43′ pigments to longer wavelength-absorbing pigments in the core antenna. A decrease in the $\Delta A_{681}/\Delta A_{703}$ ratio from 8.7 in the 0.95 ps spectrum to 2.3 in the 9 ps spectrum reflects the spectral shift of the low-energy absorbing species as in the PSI trimer. It should be noted that the $\Delta A_{681}/\Delta A_{703}$ ratio in the 9 ps spectra is equal to 1.2 and 2.3 for the PSI trimer (Figure 2A) and PSI supercomplex (Figure 2B), respectively. On the red side of the Q_y absorption band in both the PSI trimers and the PSI supercomplexes (Figure 1), the kinetics are very similar (data not shown). The overall decay of the excitation in the antenna of the CP43′−PSI supercomplex is complete within 100 ps (Figure 3B). The residual photobleaching at 110 ps is due to P700 photooxidation.

Global Analysis of the Transient Absorption Kinetics

Fast Energy Equilibration Phases. Figure 4 presents decay-associated spectra (DAS) obtained after global analysis of kinetic data recorded on the 10 ps time scale for the PSI trimer (Figure 4A) and PSI supercomplex (Figure 4B). In the PSI trimer on this time scale, the transient absorption kinetics are best fitted with three exponential components describing three kinetic processes with lifetimes of 0.45, 3.62, and >10 ps (Figure 4A). The shape of the 0.45 ps DAS is characteristic of sub-picosecond energy transfer from the Chl *a* species absorbing around 665 nm to the spectral forms of closely located Chl *a* molecules contributing to the red slope of the absorption band. Positive amplitudes in this DAS indicate a rise of the PB band with an absorption maximum around 687−690 nm. A 3.6 ps DAS in Figure 4A is ascribed to the picosecond energy redistribution process involving a pool of the long wavelength-absorbing pigments in the PSI core. Similar time constants of these two energy equilibration processes were reported for the PSI core antenna in *Synechocystis* sp. PCC6803 (*24*−*27*). The kinetic phase with a lifetime longer than 10 ps represents an overlap of two processes, excitation trapping and P700 photooxidation.

For the PSI supercomplex, the global analysis of the kinetic data on the same time scale revealed three exponential components with lifetimes of 0.36, 3.0, and >10 ps (Figure 4B). The maximum of the positive part of the 0.36 ps DAS is blue-shifted to 681 nm as compared to that in the PSI trimer (Figure 4A). The positive band of the 0.36 ps DAS (Figure 4B) is broad with a shoulder extending to the red absorption region, indicating that this part originates from the PSI trimer dynamics. The excitation decay part (negative amplitudes) of the 3 ps DAS in the PSI supercomplex is significantly different from that observed for the PSI trimer dynamics. These differences are due to coupling of CP43′, while the positive parts of the DAS with picosecond lifetimes reflect the involvement of the red-absorbing Chls of the PSI trimer in the spectral equilibration. The third component required to fit the kinetic data on the 10 ps time scale represents the sum of the trapping kinetics and P700 photooxidation. In the PSI supercomplex dynamics, this component has an increased $\Delta A_{681}/\Delta A_{703}$ ratio and extended PB in the region of CP43′ absorption as compared to a similar component in the PSI trimer dynamics (Figure 4A).

Absorption Changes Resulted from the Coupling of CP43′ to the PSI Trimer. The shape of the broad negative part of the 3 ps DAS in Figure 4B suggests an additional kinetic process occurred in the CP43′−PSI supercomplex, which is not resolved spectrally by global analysis because of time overlap with the picosecond equilibration in the core antenna of the PSI trimer.

In attempts to resolve this additional excitation dynamics in the spectral region of CP43′ absorption, we subtracted the kinetic data that have accumulated for the PSI trimer from the data that have accumulated for the PSI supercomplex. This subtraction involved all spectral curves detected

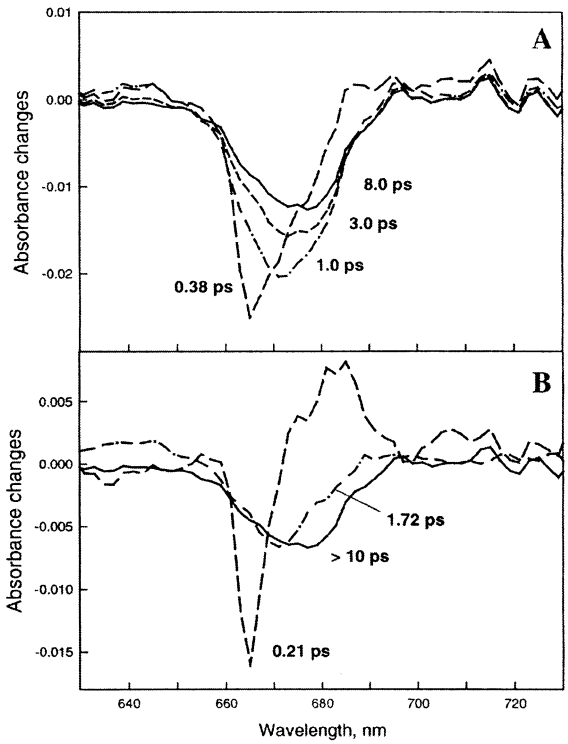

FIGURE 5: (A) Transient difference absorption spectra ($\Delta\Delta A$) resulting from subtraction of the PSI trimer kinetics from the CP43′−PSI supercomplex kinetics. The spectra are shown at different representative pump−probe delays: 0.38 (− − −), 1.0 (−•−), 3.0 (- - -), and 8.0 ps (—). See the text for a description of the subtraction normalization procedure. (B) Decay-associated spectra obtained after global analysis of the transient difference absorption spectra ($\Delta\Delta A$). The data are best fit with three exponential components with lifetimes of 0.2, 1.7, and >10 ps.

with pump−probe delays from 0 to 10 ps. The region of the absorption spectrum above 695 nm in both samples is largely contributed by the absorption of Chls in the PSI trimer (Figure 1); therefore, two sets of data were normalized per rise of the photobleaching of the low-energy Chls in the PSI antenna. The difference transient spectra ($\Delta\Delta A$) in Figure 5A illustrate a spectral evolution of Chl *a* excitation in the region of CP43′ absorption. Progressive spectral shifts in this region indicate spectral equilibration on at least two time scales, sub-picosecond and picosecond. The global analysis of the spectra resolves two energy transfer processes with lifetimes of 0.2 and 1.7 ps (Figure 5B) and the longer-living state that originates from both the photochemical trapping and an excitation decay in the CP43′ due to slower energy transfer processes. The shape of the 0.2 ps DAS is indicative of energy transfer from Chls absorbing in the region of the excitation (665 nm) to the Chl species with a maximum absorption at 681 nm. Similar spectral shifts are observed in 0.36 ps DAS in the PSI supercomplex (Figure 4B). The decay part of the 1.7 ps DAS has a maximum at 671 nm and corresponds to the blue slope of the decay part of the 3.0 ps DAS in the CP43′−PSI supercomplex (Figure 4B).

Excitation Trapping and P700 Photooxidation. Figure 6 presents results of the global analyses of the kinetic data on the time scale of 100 ps. For both PSI trimers (Figure 6A) and PSI supercomplexes (Figure 6B), the data are satisfactorily fitted with two phases of the exponential decay, excitation trapping and the state with a lifetime significantly longer than 100 ps. For the PSI trimer, the exponential component that we ascribed to the excitation trapping has a lifetime of 20 ps. This time is well-established for reaction center trapping in the PSI from *Synechocystis* sp. PCC6803 (*20*, *21*). The 20 ps DAS has a maximum ΔA at 686 nm and a broad shoulder extending from 695 to 720 nm. In the blue spectral region, the spectrum crosses zero at 673 nm. A positive part of the 20 ps DAS is due to excited state absorption. The nondecaying component in Figure 6A bears spectroscopic features of the P700 photooxidation such as a broad photobleaching around 700 nm, a positive ΔA band at 690 nm, and photobleaching bands at 670−680 nm.

In the CP43′−PSI supercomplex, the global analysis based on two-exponential component fit reveals the trapping DAS with a lifetime of ∼25 ps and a ND component (Figure 6B). The 25 ps DAS is characterized by a ΔA maximum at 684 nm and has a broad shoulder in the 695−720 nm region. However, the $\Delta A_{684}/\Delta A_{703}$ ratio in the 25 ps DAS obtained for the PSI supercomplex is 3 times larger than the $\Delta A_{686}/\Delta A_{703}$ ratio in the 20 ps DAS obtained for the PSI trimer. The observed asymmetry of the 25 ps DAS is due to the ΔA extended to the region of CP43′ absorption with the spectrum crossing zero at 660 nm. In the global analysis, the shape of this trapping DAS showed invariability with a change in the lifetime fixed in the 25−45 ps region in the two-component fit (Figure 6B). Since we could not exclusively eliminate

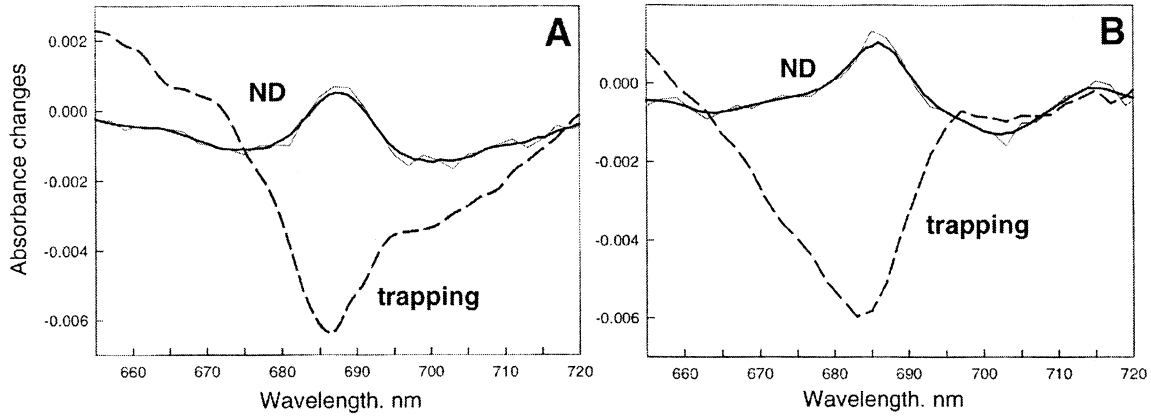

FIGURE 6: Decay-associated spectra (DAS) obtained after global analysis of transient kinetics on the 110 ps time scale with excitation at 665 nm of PSI trimers (A) and the CP43′−PSI supercomplex (B). The two-component fit with free parameters results in the trapping DAS (− − −) with lifetimes of 20 and 25 ps for the PSI trimer and PSI supercomplex, respectively, and the nondecaying component (thin solid line and thick smoothed solid line) representing largely the P700 photooxidation.

Table 1: Lifetimes (τ_i, ns) and Relative Amplitudes (A_i, %) of Exponential Decay Components of Fluorescence Kinetics Measured by SPC at Room Temperature in PSI Trimers and CP43′−PSI Supercomplexes from *Synechocystis* sp. PCC6803 (λ_{exc} = 600 nm)

		PSI trimers					PSI supercomplexes				
		$i=1$	$i=2$	$i=3$	$i=4$	χ^2	$i=1$	$i=2$	$i=3$	$i=4$	χ^2
670 nm	τ_i	0.020	0.121	1.24	4.36	1.058	0.040	0.378	1.302	4.08	1.025
	A_i	77.5	5.5	14.9	2.1		90.5	2.6	6.1	0.8	
680 nm	τ_i	0.023	0.208	1.264	5.021	1.079	0.042	0.641	1.533	5.151	1.044
	A_i	92.5	1.3	4.4	1.8		94.6	1.7	2.8	0.9	
685 nm	τ_i	0.024	0.220	1.357	5.280	1.103	0.040	0.510	1.304	4.531	1.06
	A_i	93.9	2.4	2.9	0.8		96.1	1.0	2.3	0.6	
720 nm	τ_i	0.033	0.317	1.372	4.710	1.158	0.049	0.576	1.479	4.801	1.077
	A_i	95.4	0.7	3.7	0.2		94.4	2.5	2.9	0.2	

the annihilation in the transient absorption measurement of the CP43′−PSI supercomplexes with ~500 Chl *a* molecules (see the Discussion), we used the trapping time resulting from SPC measurements (43 ± 4 ps; see below) in the global analysis of transient absorption data obtained for the CP43′−PSI supercomplex. In a three-component fit with the trapping time fixed at 40 ps (data not shown), we obtained a 10 ± 2 ps exponential component with a shape corresponding to the long-lived decay component in Figure 5B, while the shape of the 40 ps trapping DAS was largely similar to the shape of the overall trapping component in the PSI trimer (Figure 6A).

The ND spectrum in the global analyses of the CP43′−PSI data has features largely similar to those of the ND spectrum obtained for the PSI trimer (Figure 6A,B), although some contributions from uncoupled pigments excited around 660−670 nm could be expected. For both PSI trimers and CP43′−PSI supercomplexes, we observed flash-induced kinetics of the P700 photooxidation recovery on the millisecond time scale (data not shown).

Time-Resolved Fluorescence

Kinetics. We used time-correlated single-photon counting as a sensitive tool for testing the energy coupling in the CP43′−PSI supercomplex. Figure 7 shows typical kinetic traces of the fluorescence in both PSI trimers (curves 1) and CP43′−PSI supercomplexes (curves 2) detected at 720 (Figure 7A), 685 (Figure 7B), and 670 nm (Figure 7C). Thick solid lines represent the fits of the fluorescence decay with a sum of exponential components based on the convolution of the observed kinetics and the instrument response function (IRF) (curves 3). Table 1 presents the results of the single-wavelength analysis with lifetimes and relative amplitudes of the four exponential components required to fit the data. At 720 and 685 nm, the kinetics of the fluorescence decay are largely similar in both the PSI trimer and PSI supercomplex. The emission decays with a dominant (94−96% relative amplitudes) exponential component with lifetimes of 25 ± 6 ps for the PSI trimer and 43 ± 4 ps for the PSI supercomplex. Because of the high signal-to-noise ratio and the absence of singlet−singlet annihilation, we consider these data independent evidence that the overall excitation decay in the CP43′−PSI supercomplex has a somewhat longer lifetime than that in the PSI trimer. Table 1 shows that intermediate and long-lived exponential components for the PSI trimer have lifetimes of 0.12−0.32, 1.2−1.4, and 4.3−5.3 ns. Similar components for the CP43′−PSI supercomplex have lifetimes of 0.4−0.6, 1.3−1.5, and 4.1−5.2 ns. Overall, these components have relative amplitudes of <5% at 680−720 nm and can be ascribed to a small amount of uncoupled pigments or sample heterogeneity.

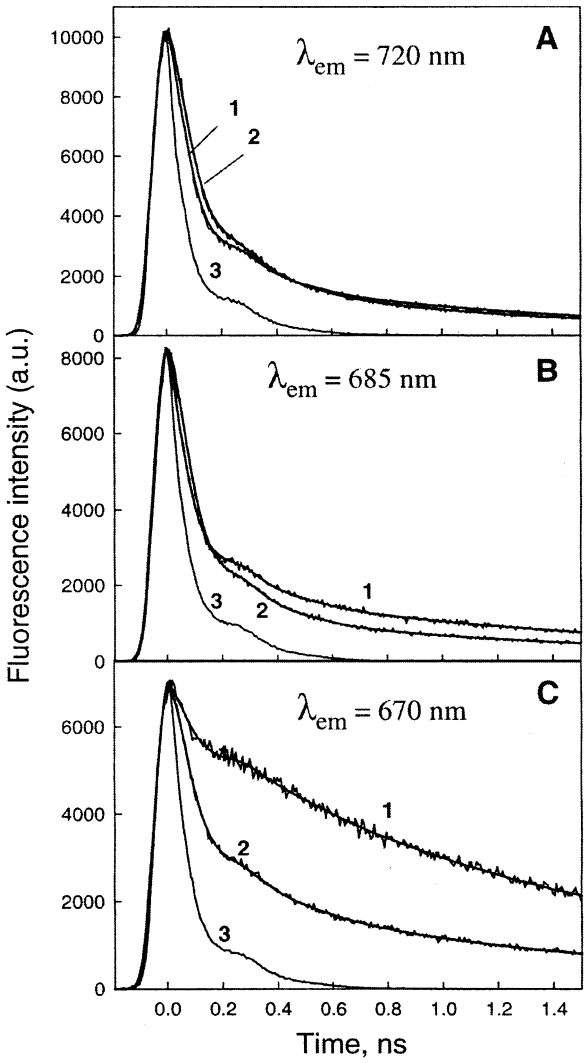

FIGURE 7: Fluorescence kinetics measured by time-correlated single-photon counting (SPC) in the PSI trimers (1) and CP43′−PSI supercomplex (2) at room temperature and with excitation at 600 nm: (A) λ_{em} = 720 nm, (B) λ_{em} = 685 nm, and (C) λ_{em} = 670 nm. The instrument response function (IRF) (3) is 100 ps. Amplitudes are normalized to the maximum count. See Table 1 for results of single-wavelength analysis of the fluorescence decay based on convolution of the observed kinetics and the IRF.

Fluorescence Decay-Associated Spectra. The spectral profile of different phases of the fluorescence decay was obtained from the global analysis of the fluorescence kinetics detected on the time scale of 10 ns in the 640−780 nm spectral region with 5 or 10 nm steps.

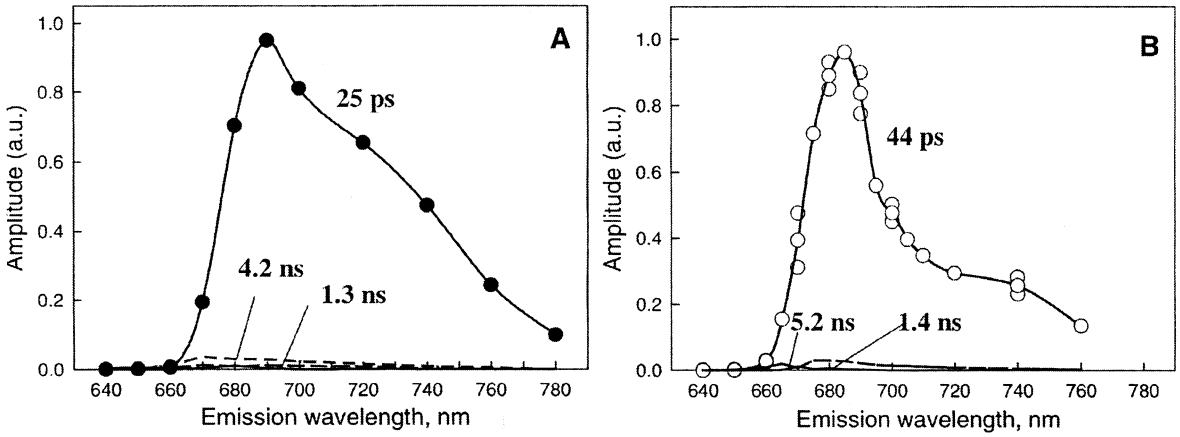

FIGURE 8: Fluorescence decay-associated spectra obtained from a four-component global fit of the fluorescence decays upon excitation at 600 nm at room temperature for PSI trimers (A) and the CP43′−PSI supercomplex (B). See explanations in the text.

Figure 8 shows fluorescence decay-associated spectra (FDAS) resulting from a four-component global fit of the emission kinetics upon excitation at 600 nm at room temperature for PSI trimers (A) and CP43′−PSI supercomplexes (B). The quality of the global fit was judged by weighted residuals and the global χ^2 parameter. The fit amplitudes were scaled to the steady state fluorescence intensity by setting the sum of the products of the amplitudes and the lifetimes equal to the intensity, $\sum_i A_i\tau_i$, at each detection wavelength. Figure 8 illustrates significantly different spectral profiles of the dominant trapping FDAS in the PSI trimers and CP43′−PSI supercomplexes. A 25 ps FDAS detected in the PSI trimer has a maximum of fluorescence decay at 685−690 nm. In this spectrum, the ratio of the amplitude at 690 nm and that at 720 nm is ∼1.5. A 44 ps FDAS detected in the CP43′−PSI supercomplex has a maximum at 680−685 nm and an F_{685}/F_{720} ratio of 3.3, indicating a blue shift and a significant relative increase in the amplitudes of the excitation trapping FDAS in the spectral region of fluorescence of CP43′.

DISCUSSION

How Strong Is CP43′ Energetically Coupled to the PSI Trimer? We have conducted the first time-resolved energy transfer studies on the CP43′−PSI supercomplex induced in the cyanobacterium *Synechocystis* sp. PCC6803 when grown in iron deficient growth medium. Data recorded by transient absorption spectroscopy using excitation at 665 nm show that the excitation of Chl *a* in the CP43′−PSI supercomplex completely decays within 100 ps, resulting in the formation of $P700^+$ (Figures 2 and 3). Use of single-photon counting fluorescence, which is very sensitive to the presence of energetically uncoupled pigments, independently demonstrates (Figures 7 and 8 and Table 1) that the vast majority of the excited states (>95%) decay on the time scale of tens of picoseconds, suggesting a ≤5% loss of excitation energy due to uncoupled or damaged complexes. This supports the general conclusion that the extra ring of CP43′ around the PSI trimer in the supercomplex is energetically efficiently coupled to the antenna network of the PSI core.

The data of Figure 2 provide evidence that the energy transfer dynamics of the CP43′−PSI supercomplex are comparable with energy transfer processes that occur in the Chl *a* network of the PSI trimer antenna. Observed subpicosecond dynamics in the PSI trimer are characteristic of energy transfer processes between Chl *a* molecules in clusters of the core antenna. Transient absorption spectra as well as kinetics of the fluorescence decay detected for the PSI trimer are in good agreement with those reported previously for PSI from *Synechocystis* sp. PCC6803 (*24*−*27*) and other cyanobacterial species (*21*).

The increases of the photobleaching Δ*A* band around 690−710 nm in the 2−4 ps DAS in both the PSI trimer and CP43′−PSI supercomplex (Figure 4) have similar spectral profiles. The observed absorption changes in this part of the spectrum originate from energy transfer dynamics in the PSI trimer, specifically, from the picosecond redistribution that involves long wavelength-absorbing Chls. The number of these "red pigments" in the PSI trimers from *Synechocystis* sp. PCC6803 is smaller than the number in the PSI from *S. elongatus*. As a result, the excitation dynamics in the PSI trimers and monomers are largely similar in *Synechocystis* sp. (*20*) in contrast to those in *S. elongatus*. Global analysis of the kinetic data on the time scale of 100 ps for the CP43′−PSI supercomplex (Figure 6B) revealed that both photochemical trapping and P700 photooxidation spectra are consistent with the functional part of the supercomplex being contained within the PSI. We can conclude, therefore, that both time-resolved absorption and fluorescence measurements as well as our earlier results on steady state fluorescence (*10*, *13*) indicate that the CP43′ antenna ring of the supercomplex is efficiently coupled to the PSI core and in this way significantly increases the absorption cross section of the reaction center. Recently, Boekema and co-workers (*17*) came to similar conclusions based on the analysis of light saturation curves of absorbance changes at 703 nm of PSI and CP43′−PSI (PSI−IsiA according to the labeling of the authors) complexes from the cyanobacterium *Synechococcus* sp. PCC7942.

Energy Transfer from CP43′ to the PSI Core. Energy coupling of CP43′ to the PSI trimer suggests the presence of energy transfer processes from the outer CP43′ ring to the PSI trimer. Despite the blue shift of the CP43′ absorption spectrum relative to the absorption band of the PSI trimer (Figure 1), there is a substantial spectral overlap that complicates the analysis of the data. Comparison of transient absorption spectra in the PSI trimer and the CP43′−PSI supercomplex (Figure 2) and transient kinetics at 665 nm

(Figure 3) shows that the most significant changes in the PSI supercomplex dynamics are observed within the first several picoseconds after the excitation in the spectral region of CP43′ absorption. Therefore, subtraction of the time-resolved spectra detected for the PSI trimer for the CP43′−PSI supercomplex will reveal the excitation dynamics that resulted from the coupling of CP43′ to the PSI trimer. For the subtraction normalization procedure, we used the fact that the number of low-energy pigments and P700 is constant in both complexes. We assumed that no more long wavelength-absorbing red pigments were induced upon coupling of CP43′ to the PSI trimer, because the estimated distances between the outer ring and the surface of the PSI trimer (*16*) are not sufficiently short to induce excitonic interactions, the most common cause for the red spectral shifts. The result of this subtraction shown in Figure 5A indicates the transient absorption spectra following the excitation of Chl *a* at 665 nm in the region of CP43′ absorption with a maximum at 672 nm. The observed absorbance changes reflect both the excitation dynamics within the CP43′ ring and the energy transfer induced by the coupling of the outer ring to the PSI trimer. The global analysis of the spectra resolves three kinetic components with lifetimes of 0.2, 1.7, and >10 ps (Figure 5B). Although the structure of CP43′ is unknown, CP43 from the PSII can be used as a working model for the CP43′ structure (*10*, *13*, *16*). If we assume that the coupling of CP43′ to the PSI trimer does not affect the structure of the PSI core antenna, then the majority of the sub-picosecond dynamics in the $\Delta\Delta A$ spectra (0.2 ps process) might originate from the energy transfer within the cluster of Chls in the CP43′ overlapped with excitation delocalization over the CP43′ ring. Recently, a time-resolved study of the isolated CP43 from the PSII at 77 K (*28*) reported on the 0.4 ps energy transfer due to the excitation hopping within the stromal layer of Chls in CP43. We cannot distinguish, however, between sub-picosecond processes within individual CP43′ subunits and between neighboring CP43′ subunits in the ring. The time-resolved study of the individual CP43′ is in progress.

Since the most significant changes in the excitation dynamics of the CP43′−PSI supercomplex are observed within several picoseconds of the excitation at 665 nm (Figure 2), the 1.7 ps DAS (Figure 5B) most probably reflects the equilibration processes in the CP43′ itself as well as the CP43′−PSI energy transfer processes induced by the coupling. In the study of the isolated CP43 from PSII (*28*), the equilibration process with a lifetime of 2−4 ps was ascribed to the energy transfer between Chls in different layers of the individual complex. However, the kinetic processes observed on the picosecond time scale in the spectral region of the CP43′ absorption are more complicated (Figures 2B and 5B). The ratio of sub-picosecond and picosecond energy transfer processes in the ring depends on the strength of the coupling between the individual CP43′ proteins in the ring and the distances from the ring to the PSI trimer. On the basis of the available three-dimensional (3D) cryo-EM structural model of the PSI supercomplex (*16*), specific clusters of Chl *a* bound to PsaA, PsaB, and PsaJ in the PSI trimer are thought to be in contact with Chl *a* clusters of CP43′ with the distances between the ring and the PSI trimer ranging from 20 to 25 Å. The extent of energy delocalization in the CP43′ ring is not possible to predict without detailed spectroscopic and structural data of the CP43′ ring. On one hand, the excitation is definitely not delocalized over the whole ring, because irregularities in the structure would result in early energy localization. In this respect, the CP43′ ring is significantly different from the light-harvesting LH2 antenna ring and the LH1−RC complex from purple bacteria (*29*, *30*). On the other hand, the energy delocalization process might compete with the energy transfer from CP43′ to the PSI core via the suggested linker chlorophylls on the periphery of PsaA, PsaB, and PsaJ subunits (*10*, *16*). Our estimations of the distance between the energy donor and acceptor in the ∼2 ps energy transfer from the CP43′ ring to the PSI trimer based on Förster theory give a distance of ∼20 Å, in good agreement with the distance estimated from the structural model.

The third kinetic component obtained in the global analysis of the $\Delta\Delta A$ spectra on the 10 ps time scale (Figure 5) has a lifetime longer than 10 ps. This DAS might reflect either the longer-living state originating largely from the photochemical trapping (see below) or the slower energy transfer process from CP43′ to the PSI core. In the three-component global analysis of the transient kinetics of the CP43′−PSI supercomplex on the 100 ps time scale, fixing of the 40 ps trapping constant results in the appearance of a kinetic phase with a lifetime of 10 ± 2 ps and the maximum of the excitation decay at 672 nm (data not shown). The available low-resolution structural model of the CP43′−PSI supercomplex (*10*, *16*) would predict both picosecond (2 ps) and slower (10 ps) energy transfer processes from the CP43′ ring to the PSI trimer. The nine energy entries suggested in the PSI trimer from 18 CP43′ complexes in the ring (*16*) constitute a 50% probability of fast energy transfer. The other 50% of the excitation in the CP43′ ring might reach the PSI trimer in an overall energy transfer. We note, however, that a detailed analysis of these kinetics requires building of the kinetic model, which is beyond the scope of this study.

Photochemical Trapping in the PSI Supercomplex. The picosecond fluorescence spectroscopy data (Figure 8) provide evidence that the dominant phase of the fluorescence decay, with lifetimes of 25 ps in the PSI trimer and 43 ps in the CP43′−PSI supercomplex, occurs from the thermally equilibrated state. A 72% increase in the antenna size in the CP43′−PSI supercomplex (*10*, *13*) results in a change in the Boltzmann distribution of the Chl *a* excitation in the whole antenna complex. This change of the thermal distribution is indicated by the blue shift of the photochemical trapping (Figures 6B and 8B) as well as the 3-fold increase in the $\Delta A_{684}/\Delta A_{703}$ ratio in the trapping DAS of the PSI supercomplex.

Results of annihilation-free single-photon counting experiments clearly indicate that the lifetime of the overall excitation decay in the antenna of the CP43′−PSI supercomplex is systematically longer than in the core antenna of the PSI trimer. At the excitation intensity level used in this study ($\sim 10^{14}$ photons pulse^{-1} cm^{-2}), we calculate that fewer than four photons were absorbed per PSI supercomplex for each laser pulse. Taking into account the fact that the absorption at 665 nm is due to both the outer antenna ring and the PSI trimer with an approximately 1:1 ratio, we find only two photons will be absorbed by each part on average. There are three monomers in the core complex, and the energy coupling among the three monomers in *Synechocystis*

is known to be weak; therefore, the PSI trimer in *Synechocystis* can be considered three weakly coupled monomers each absorbing on average two-thirds of a photon. The outer antenna ring contains 18 copies of CP43′ subunits, and the interaction between the chlorophylls from different subunits is also expected to be weak, based on comparisons with similar antenna complexes. On the basis of those facts, it is concluded that the possibility of two photons being annihilated is low and should have only minor effects on the trapping kinetics. It is important to distinguish this situation from that of other antennas such as the LH2 complex from purple bacteria where the pigments are very strongly coupled. As a result of this, annihilation effects in LH2 will be manifested at much lower doses than in the PSI reaction center with much more weakly coupled pigments. Because of the very large number of pigments in the CP43′−PSI supercomplex, it is practically not possible to completely avoid the situation where more than one photon is absorbed per complex per flash. However, because of the weak coupling that is unquestionably present in this system, the effects of multiple excitations will be significantly attenuated, especially at the early times (<10 ps) emphasized in our work.

Coupling of the outer CP43′ antenna to the PSI trimer could result in the formation of a limiting step that would shift the excitation dynamics in the PSI antenna from trap-limited to diffusion-limited. In our experiments, we did not find direct experimental evidence of the slow energy transfer processes that could significantly limit the overall excitation dynamics in the CP43′−PSI supercomplex. The suggested energy equilibration processes between CP43′ and the PSI core antenna with lifetimes of 1.7 and 10 ps are faster than the excitation trapping in the whole CP43′−PSI supercomplex (43 ps). The longer trapping time in the CP43′−PSI supercomplex reflects the fact that the entire antenna is larger so that the fraction of time that the excitation is on P700, and therefore available for trapping, is shorter.

Rapid and efficient energy transfer between the outer CP43′ antenna ring and the PSI reaction center complex in cyanobacteria makes the CP43′−PSI supercomplex significantly different from the LHCI−PSI supercomplex from higher plants and green algae where slower energy transfer processes from the peripheral LHCI antenna to the PSI core with a time scale in the range of hundreds of picoseconds were suggested (*20*, *36*). Less efficient energy coupling in the LHCI−PSI supercomplex of higher plants is probably a result of the structural adaptation of the LHCI peripheral antenna that not only extends the absorption cross section of the PSI core but also participates in regulation of excitation flows between the two photosystems as well as in photoprotection. The structural stability and very efficient energy coupling in the cyanobacterial CP43′−PSI supercomplex are adaptive responses of the cells under the conditions of low light and continuous nutrient limitations in the aquatic environment.

NOTE ADDED IN PROOF

A recent three-dimensional structure of PSII from the cyanobacterium *Thermosynechococcus vulcanus* resolved at 3.7 Å revealed 13 Chl *a* molecules in the CP43 complex (*37*). On the basis of the similarity of CP43 and CP43′, this will constitute an 81% increase of the antenna size of the iron stress-induced CP43−PSI supercomplex from *Synechocystis* sp. PCC6803 as compared to the antenna size of the PSI trimer. A low-temperature steady state spectroscopy study of the CP43−PSI supercomplex from the cyanobacterium *Synechococcus* PCC7942 predicted 16 Chl *a* molecules per CP43′ (*38*).

REFERENCES

1. Blankenship, R. E. (2002) *Molecular mechanisms of photosynthesis*, Blackwell Science, Malden, MA.
2. Gantt, E. (1975) *BioSciences 25*, 781−788.
3. Glazer, A. N. (1982) *Annu. Rev. Microbiol. 36*, 173−198.
4. Martin, J. H., et al. (1994) *Nature 371*, 123−129.
5. Pakrasi, H. B., Riethman, H. C., and Sherman, L. A. (1985) *Proc. Natl. Acad. Sci. U.S.A. 82*, 6903−6907.
6. Straus, N. A. (1994) in *Molecular Biology of Cyanobacteria* (Bryant, D. A., Ed.) pp 731−750, Kluwer Academic Press, Dordrecht, The Netherlands.
7. Guikema, J., and Sherman, L. A. (1983) *Plant Physiol. 73*, 250−256.
8. Laudenbach, D., and Strauss, N. A. (1988) *J. Bacteriol. 170*, 5018−5026.
9. Burnap, R. L., Troyan, T., and Sherman, L. A. (1993) *Plant Physiol. 103*, 893−902.
10. Bibby, T. S., Nield, J., and Barber, J. (2001) *J. Biol. Chem. 276*, 43246−43252.
11. Bricker, T. M., and Frankel, L. K. (2002) *Photosynth. Res. 72*, 131−146.
12. Sandström, S., Park, Y.-Y., Öquist, G., and Gustafsson, P. (2001) *Photochem. Photobiol. 74*, 431−437.
13. Bibby, T. S., Nield, J., and Barber, J. (2001) *Nature 412*, 743−745.
14. Jordan, P., Fromme, P., Witt, H. T., Klukas, O., Saenger, W., and Krauss, N. (2001) *Nature 411*, 909−917.
15. Zouni, A., Witt, H.-T., Kern, J., Fromme, P., Krauss, N., Saenger, W., and Orth, P. (2001) *Nature 409*, 739−743.
16. Nield, J., Morris, E. P., Bibby, T. S., and Barber, J. (2003) *Biochemistry* (in press).
17. Boekema, E. J., Hifney, A., Yakushevska, A. E., Piotrovski, M., Keegstra, W., Berry, S., Michel, K.-P., Pistorius, E. K., and Kruip, J. (2001) *Nature 412*, 745−748.
18. Bibby, T. S., Nield, J., Partensky, F., and Barber, J. (2001) *Nature 413*, 590.
19. Karapetyan, N. V., Holzwarth, A. R., and Rögner, M. (1999) *FEBS Lett. 460*, 395−400.
20. Melkozernov, A. N. (2001) *Photosynth. Res. 70*, 129−153.
21. Gobets, B., and van Grondelle, R. (2001) *Biochim. Biophys. Acta 1507*, 80−99.
22. Fromme, P., Jordan, P., and Krauss, N. (2001) *Biochim. Biophys. Acta 1507*, 5−31.
23. Chitnis, P. R. (2001) *Annu. Rev. Plant Physiol. Plant Mol. Biol. 52*, 593−626.
24. Savikhin, S., Xu, W., Soukoulis, V., Chitnis, P. R., and Struve, W. (1999) *Biophys. J. 76*, 3278−3288.
25. Melkozernov, A. N., Lin, S., and Blankenship, R. E. (2000) *Biochemistry 39*, 1489−1498.
26. Melkozernov, A. N., Lin, S., Blankenship, R., and Valkunas, L. (2001) *Biophys. J. 81*, 1144−1154.
27. Gobets, B., van Stokkum, I. H. M., Rögner, M., Kruip, J., Schlodder, E., Karapetyan, N., Dekker, J. P., and van Grondelle, R. (2001) *Biophys. J. 81*, 407−424.
28. de Weerd, F. L., van Stokkum, I. H. M., van Amerongen, H., Dekker, J. P., and van Grondelle, R. (2002) *Biophys. J. 82*, 1586−1597.
29. Cogdell, R. J., Isaacs, N. W., Howard, T. D., McLuskey, K., Fraser, N. J., and Prince, S. M. (1999) *J. Bacteriol. 181*, 3869−3879.
30. Sundström, V., Pullerits, T., and van Grondelle, R. (1999) *J. Phys. Chem. B 103*, 2327−2346.
31. Hastings, G., Hoshina, S., Webber, A. N., and Blankenship, R. E. (1995) *Biochemistry 34*, 15512−15522.
32. Melkozernov, A. N., Su, H., Lin, S., Bingham, S., Webber, A. N., and Blankenship, R. E. (1997) *Biochemistry 36*, 2898−2907.
33. Byrdin, M., Jordan, P., Krauss, N., Fromme, P., Stehlik, D., and Schlodder, E. (2002) *Biophys. J. 83*, 433−457.
34. Bricker, T. M., Morvant, J., Marsi, N., Sutton, H. M., and Frankel, L. K. (1998) *Biochim. Biophys. Acta 1409*, 50−57.

35. Causgrove, T. P., Brune, D. C., Blankenship, R. E., and Olson, J. M. (1990) *Photosynth. Res*. *25*, 1−10.
36. Croce, R., Dorra, D., Holzwarth, A. R., and Jennings, R. C. (2000) *Biochemistry 39*, 6341−6348.
37. Kamiya, N., and Schen, J.-R. (2003) *Proc. Natl. Acad. Sci. U.S.A. 100*, 98−103.
38. Andrizhiyevskaya, E. G., Schwabe, T. M. E., Germano, M., D'Haene, S., Kruip, J., van Grondelle, R., and Dekker, J. P. (2002) *Biochim. Biophys. Acta 1556*, 265−272.

BI026987U